Electronic Supplementary Information(EIS)

Synthesis of hollow GeO_2 nanostructures, transformation into Ge@C, and lithium storage properties

Li Li,[a] Kuok Hau Seng,[ab] Chuanqi Feng,[bc] Hua Kun Liu [a], *Zaiping Guo,* [* abc]

[a] *Institute for Superconducting and Electronics Materials,University of Wollongong, Wollonong,2500,Australia. Fax:+61 2 42215225; E-mail: zguo@uow.edu.au*

[b] *School of Mechanical, Materials, and Mechatronic Engineering, University of Wollongong, Wollongong,2500, Australia.*

[c] *College of Chemistry& Chemical Engineering, Hubei University, Wuhan 430062, P. R. China*

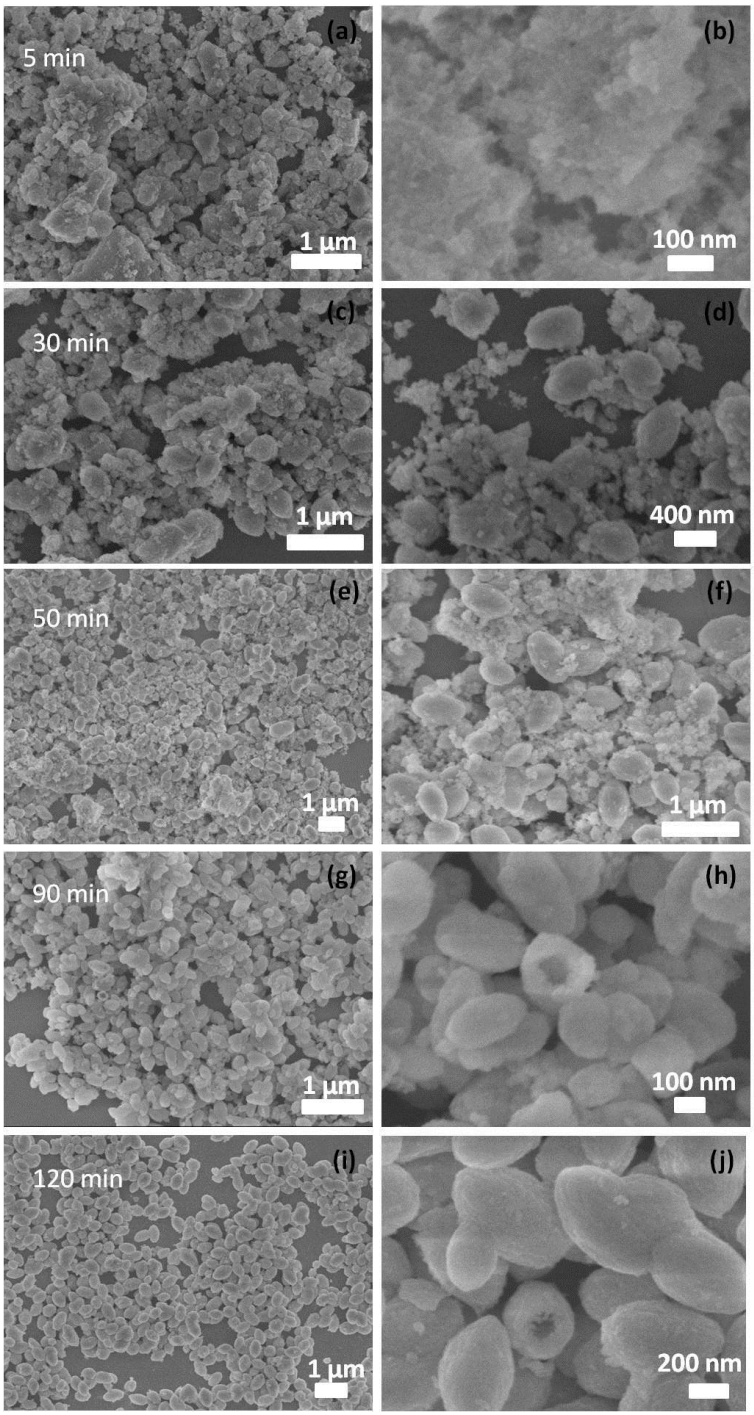

Fig. S1. FE-SEM images of GeO_2 precursors synthesized at different reaction times: (a, b) 5, (c, d) 30, (e, f) 50, (g, h) 90, (i, j) 120 min.

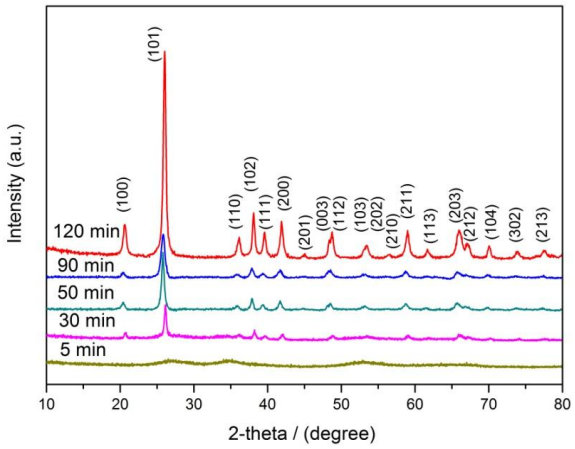

Fig. S2. X-ray diffraction patterns of GeO_2 precursors at different reaction times.

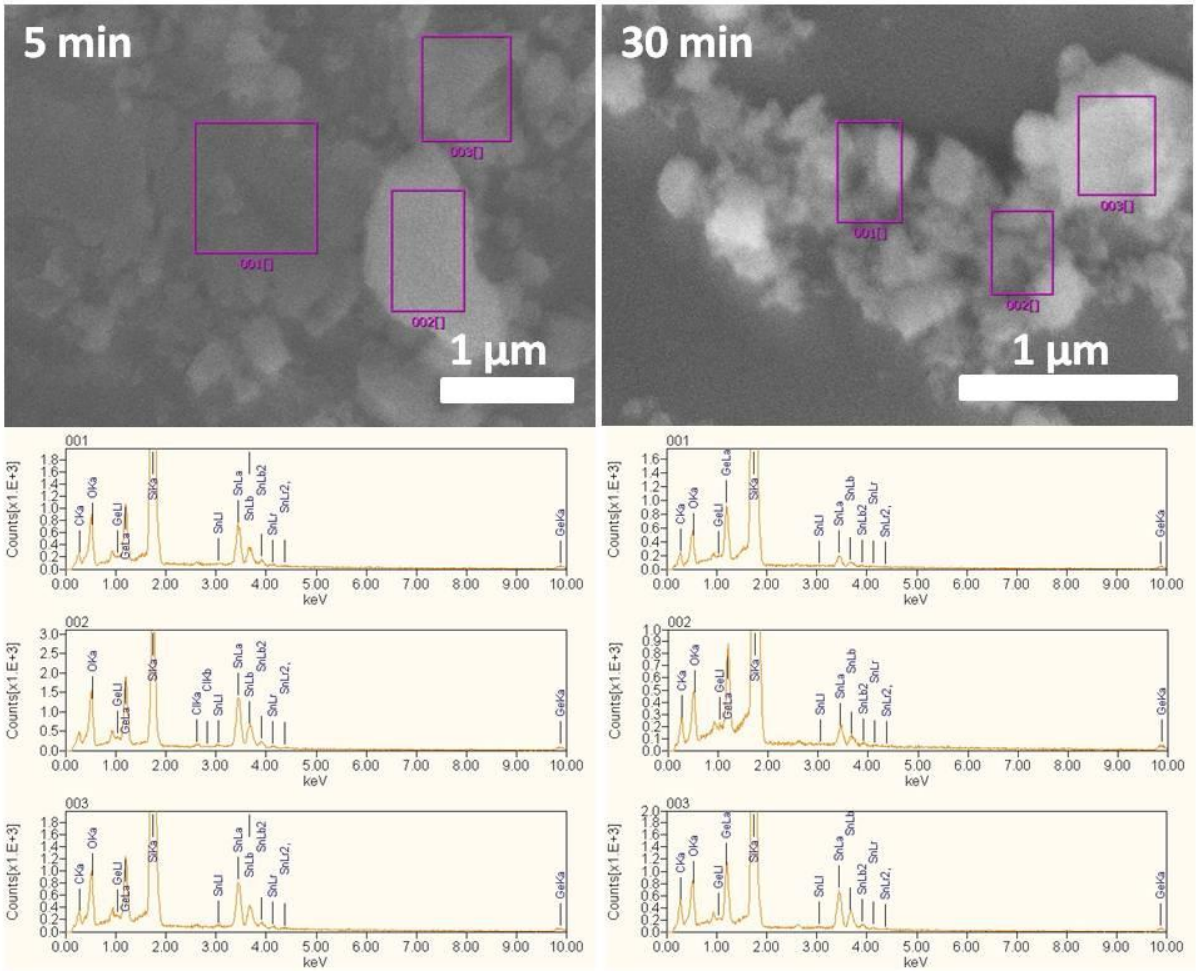

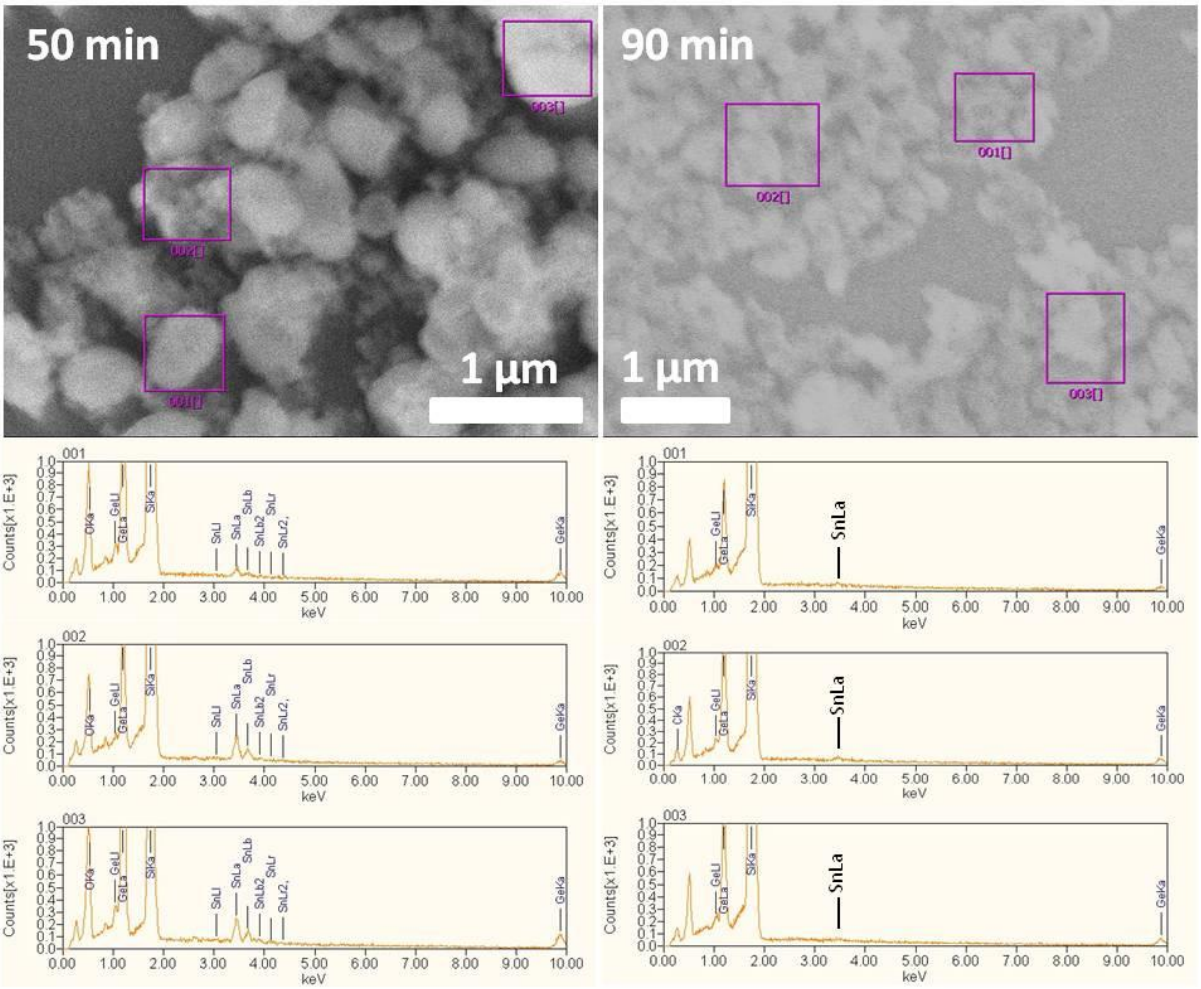
50 min
1 µm
003[]
002[]
001[]
90 min
1 µm
001[]
002[]
003[]
001
002
003
Counts[x1 E+3]
keV
OKa
GeLl
GeLa
SiKa
SnLl
SnLa
SnLb
SnLb2
SnLr
SnLz2
GeKa
SnLa

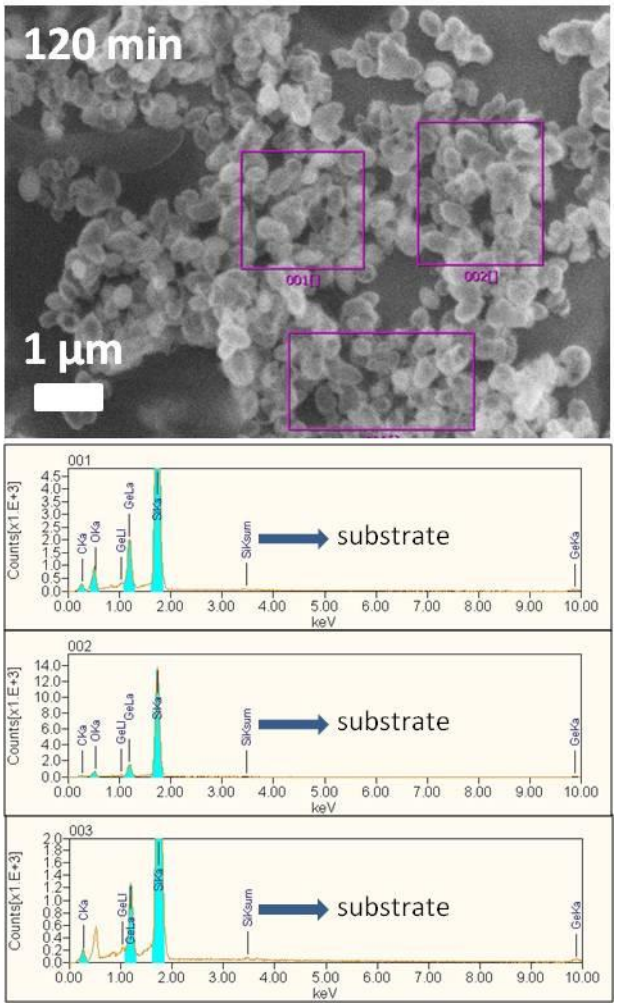

Fig. S3. EDS spectra of GeO_2 precursors at different reaction times with corresponding FE-SEM images.

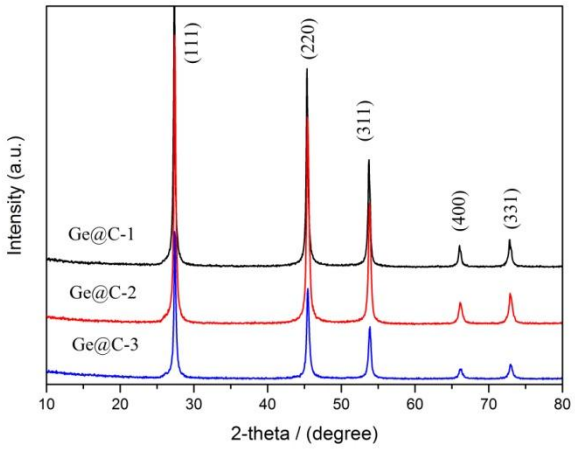

Fig. S4. X-ray diffraction patterns of Ge@C ellipsoids (Ge@C-1, Ge@C-2, Ge@C-3).

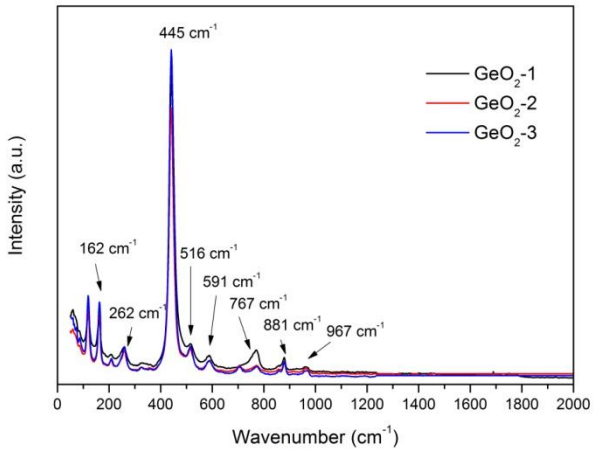

(a)

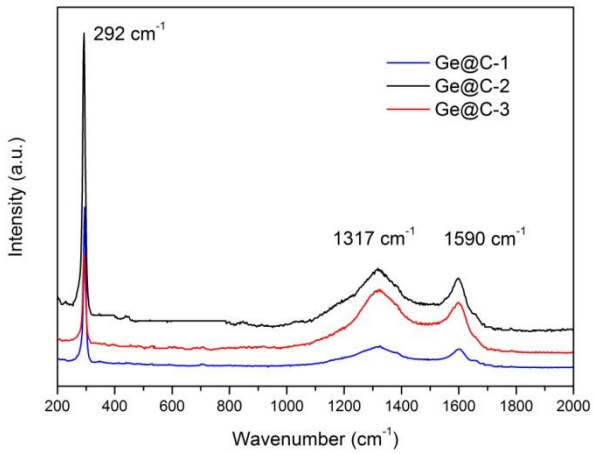

(b)

Fig. S5. Raman spectra of (a) GeO_2 precursors and (b) Ge@C.

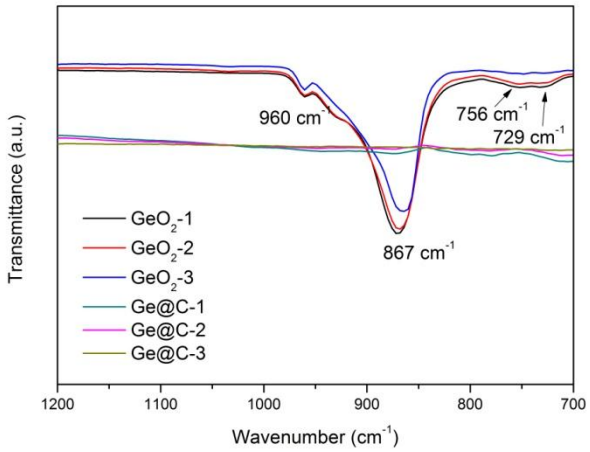

Fig. S6. FTIR spectra of GeO_2 precursors and Ge@C.

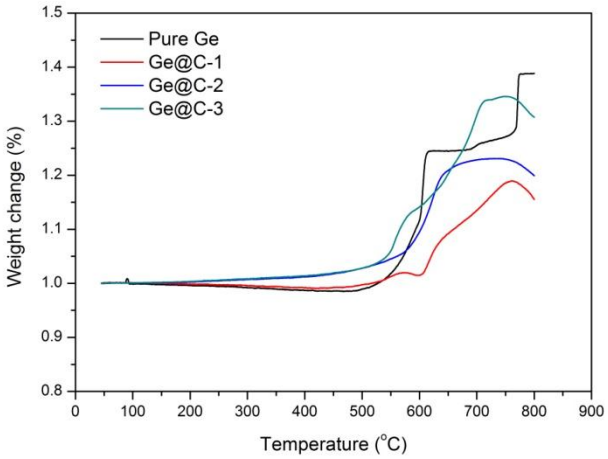

Fig. S7. TGA curves of Ge@C and pure Ge.

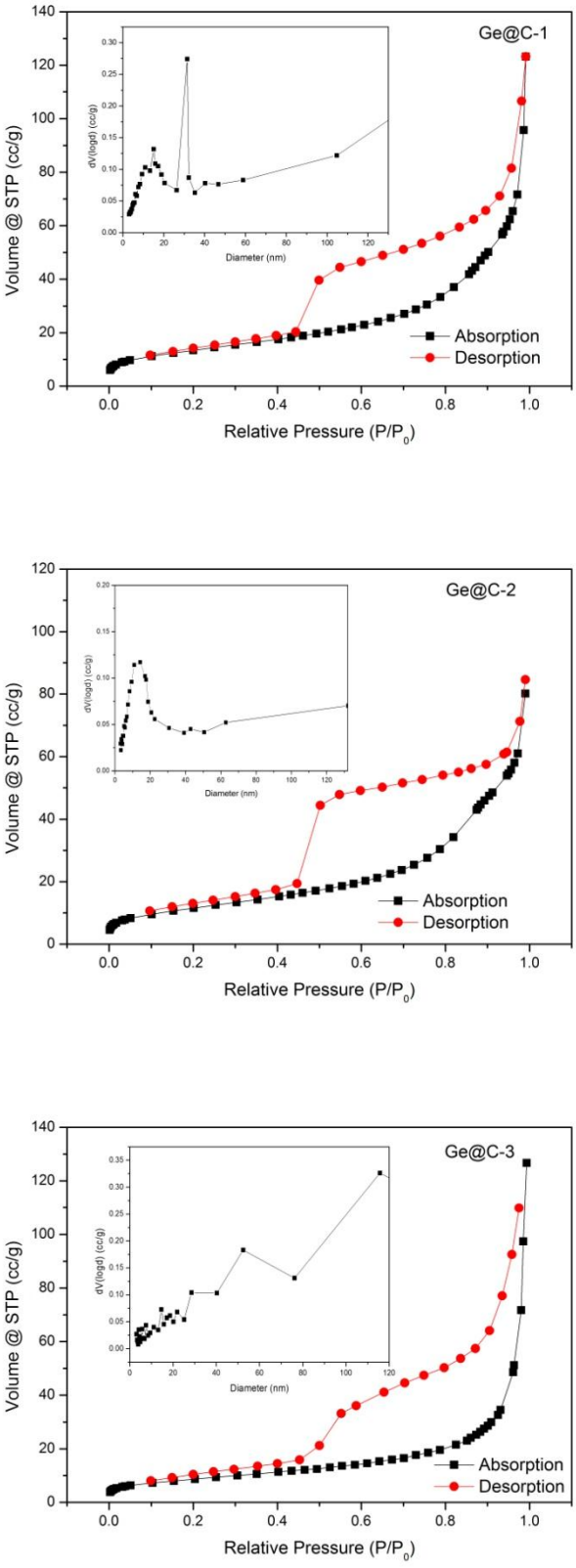

Fig. S8. Nitrogen adsorption-desorption isotherms and Barrett-Joyner-Hallenda (BJH) pore size distribution plots (inset) of hollow Ge@C ellipsoids.

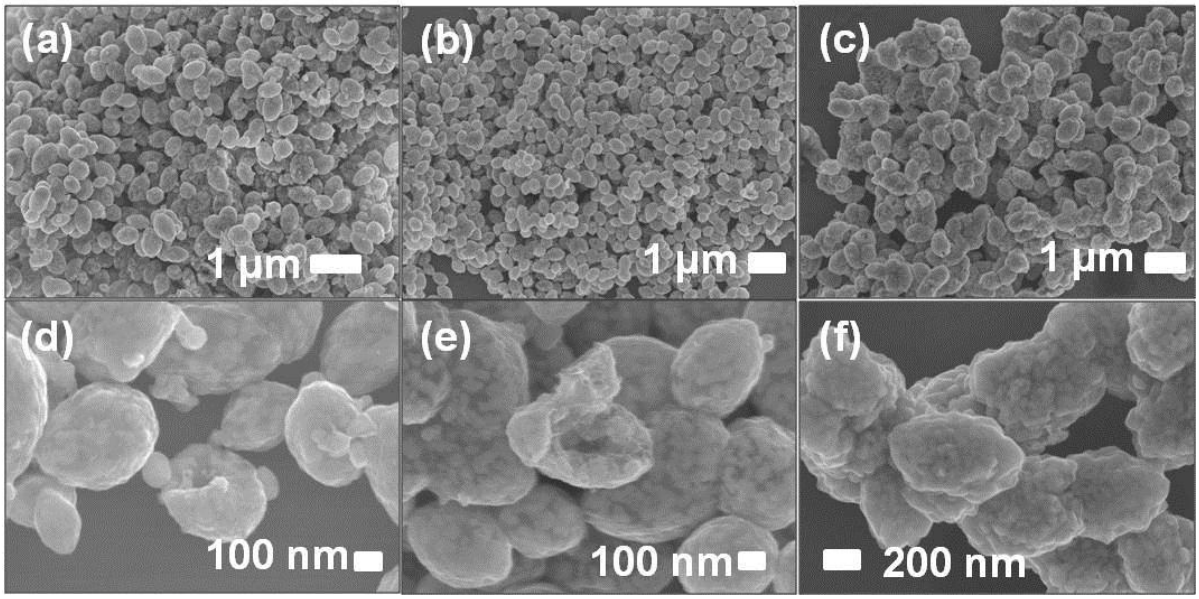

Fig. S9. FE-SEM images of (a, d) Ge@C-1, (b, e) Ge@C-2, and (c, f) Ge@C-3 samples at different resolutions.

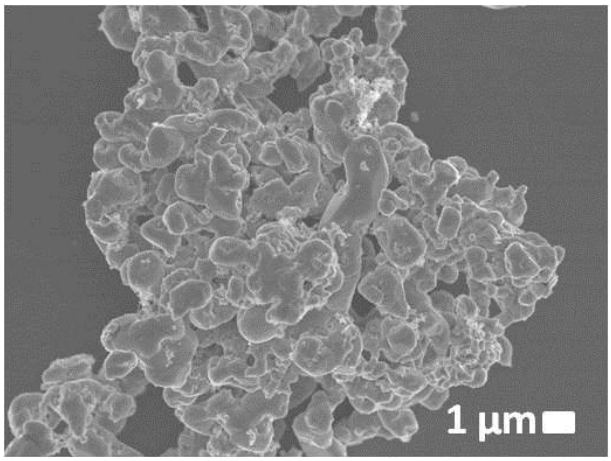

Fig. S10. FE-SEM image of pure Ge after reduction in H_2/Ar.

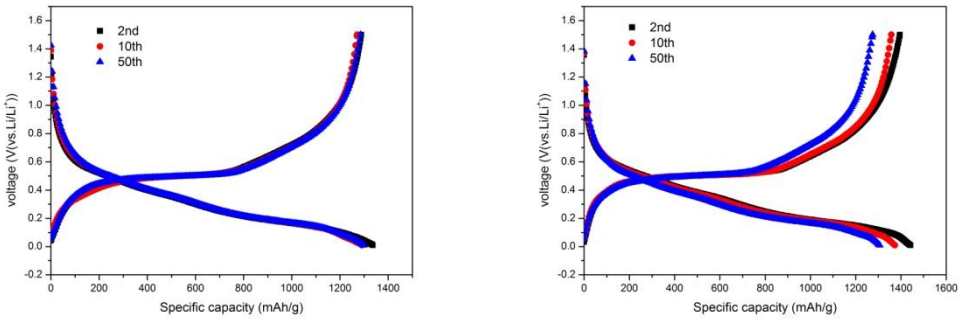

(a) (b)

Fig. S11. Voltage profiles of (a) Ge@C-1 and (b) Ge@C-3 at 2nd, 10th, and 50th cycles at 0.2 C in the range of 0.01 V to 1.5 V.

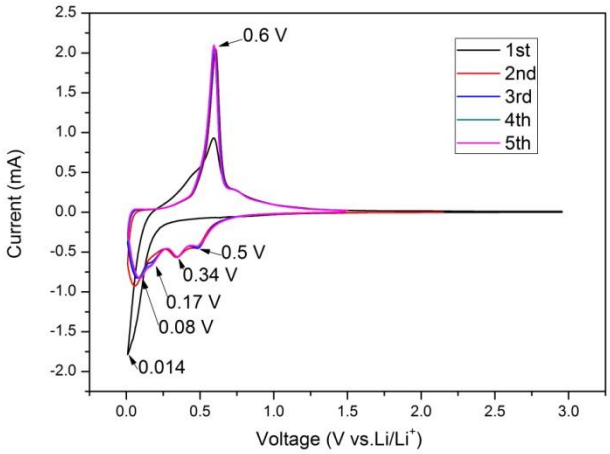

Fig. S12. Cyclic voltammograms for Ge@C-1 sample for the first 5 cycles at the scan rate of 0.1 mV/s from 0.01 V to 1.5 V.

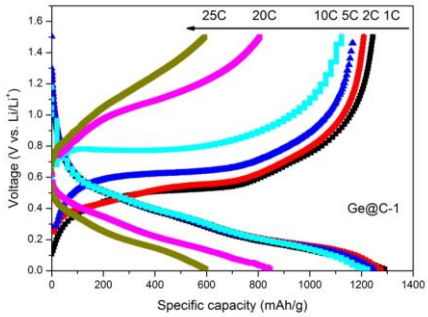

(a)

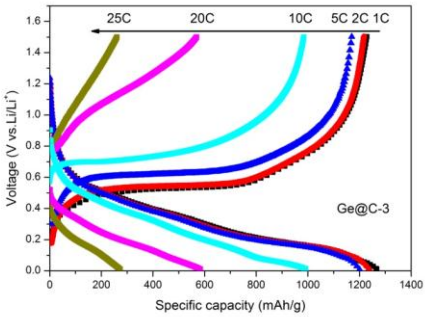

(b)

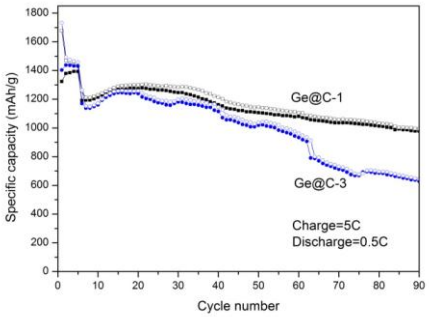

(c)

Fig. S13. Voltage profiles of (a) Ge@C-1 and (b) Ge@C-3 at different rates, (c) cycling performance of Ge@C-1 and Ge@C-3 at the 0.1 C/0.1 C charging/discharging rate for the first 5 cycles, then at the 5 C/0.5 C charging/discharging rate for the rest of the cycling.

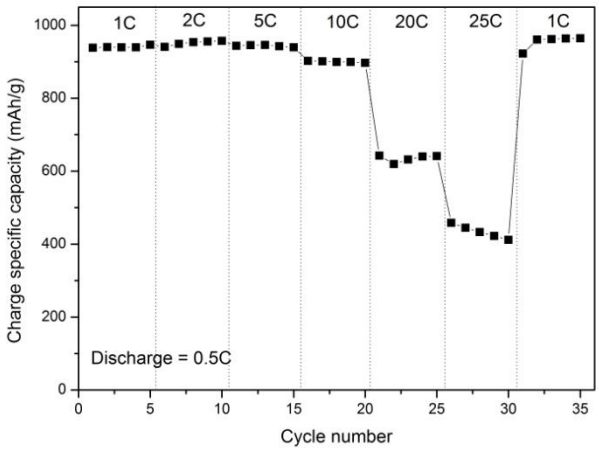

Fig. S14. Rate performance of Ge@C-4 at increasing rates from 1 to 25 C, with the discharging rate fixed at 0.5 C.

The Ge@C-4 sample was synthesized under the same conditions as Ge@C-3, except for the reaction temperature of 750 ^{o}C. From Fig. S14, we can observe that at low rates, the capacity retention is increased compared to Ge@C-3, but when the rate is increased to 20 C and 25 C, the capacity is still lower than that of Ge@C-1. This demonstrates that the enhanced electrochemical performance of Ge as anode material for LIBs is not only attributable to the amount of carbon shell, but also related to the hollow and porous structure.